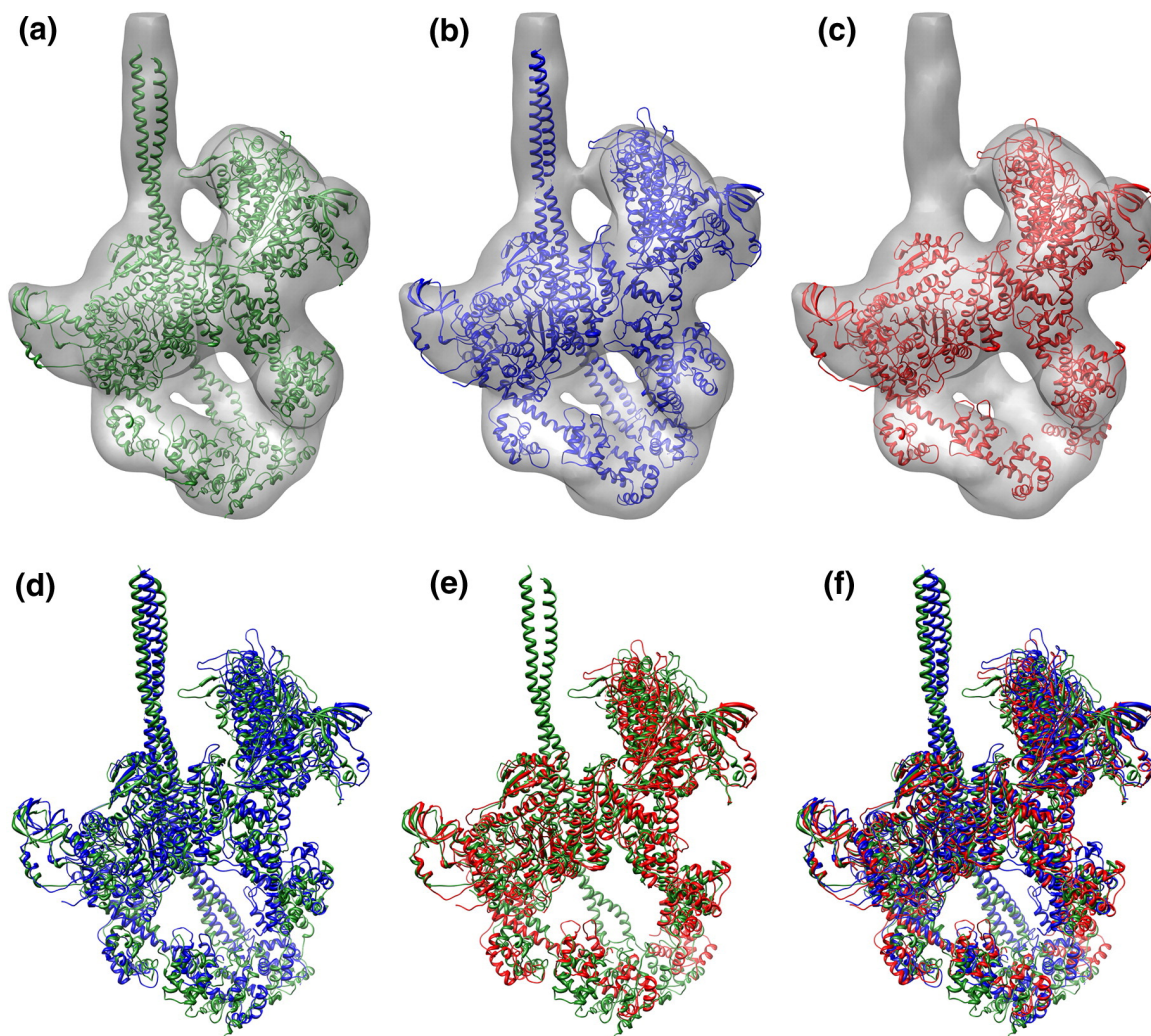# Appendix A. Supplementary Data
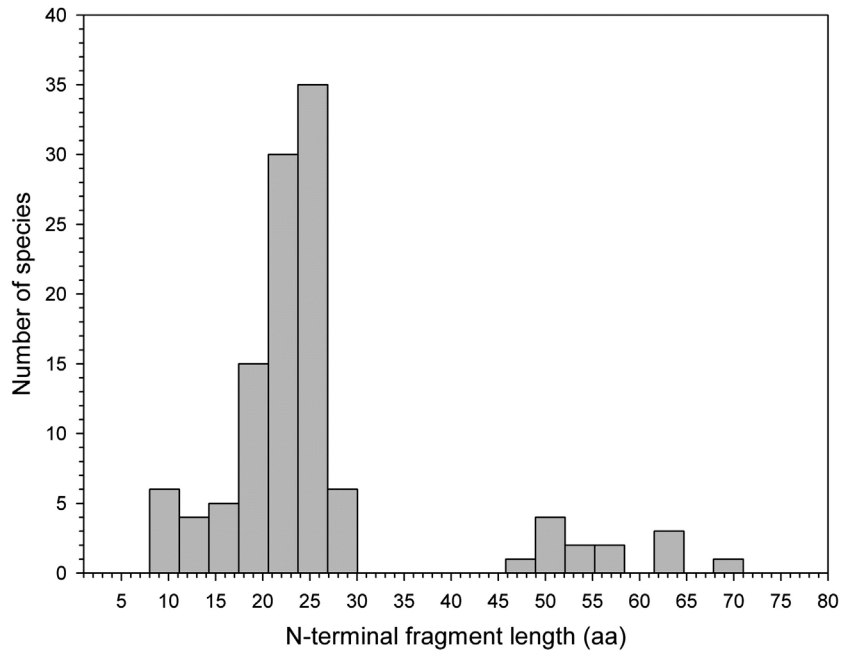
Suppl. Fig. 1. Histogram of the length of the NTF (in amino acids) for the 111 reported RLC sequences. Two NTF populations are seen, short (8–27 aa, 100 species) and long (48–71 aa, 11 species). The tarantula NTF (52 aa) belong to the class of long NTFs (Fig. 3a).

Suppl. Fig. 2. Comparison of the interacting-head atomic structure reported here. Top row shows the three structures fitted against the three-dimensional map (gray): (a) after flexible fitting (green, see Fig. 5b), (b) the previously reported by Woodhead *et al.* 200518 (blue) and (c) the initially reported by Liu et al 200316 (red). The bottom row shows the comparison between the three structures: (d) between (a) and (b), (e) between (a) and (c), and (f) between (a), (b) and (c).

(a)

(b) (c)

(d) (e) (f)
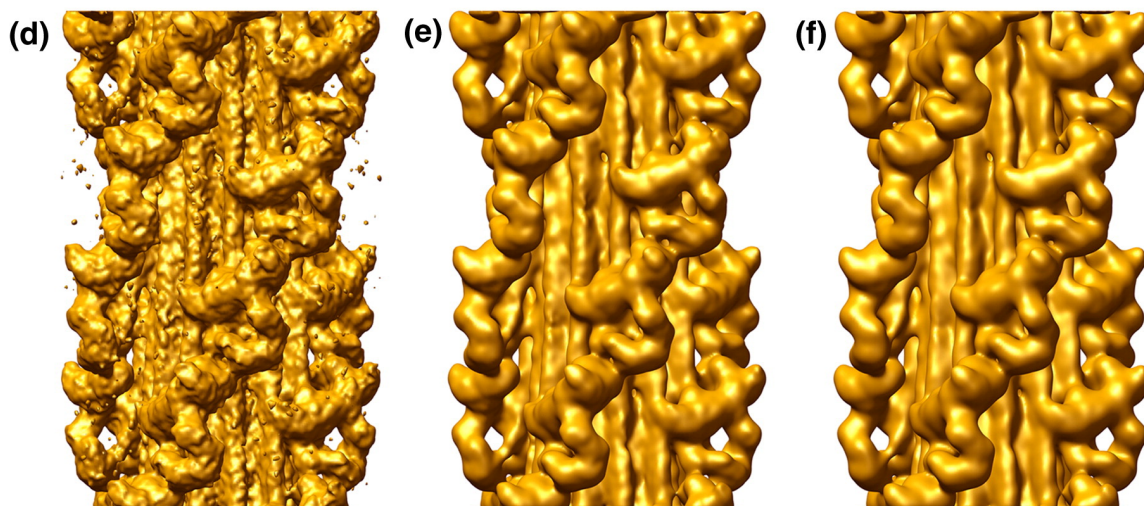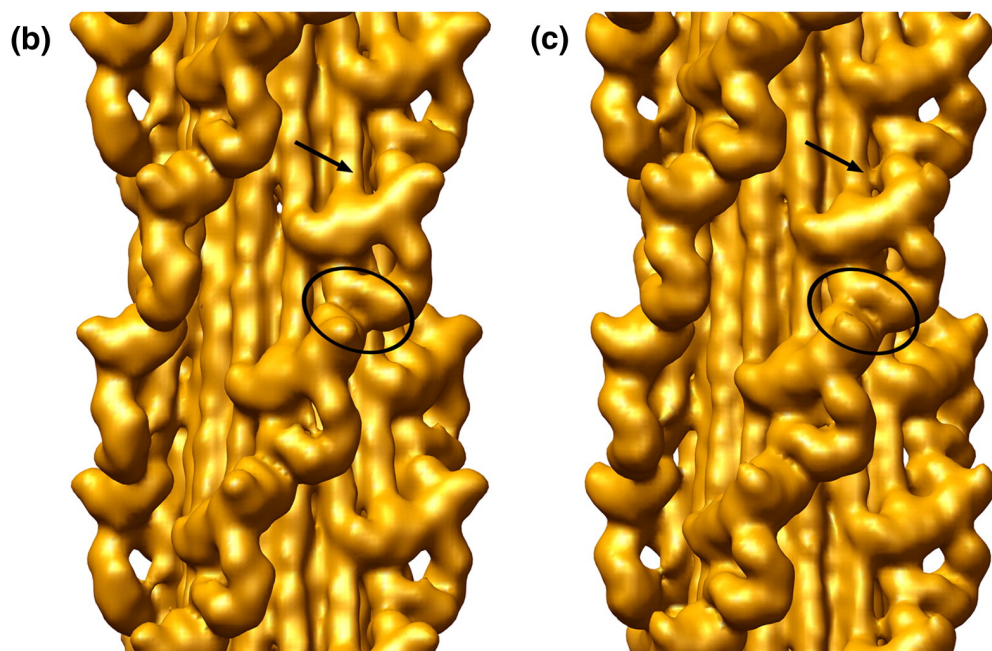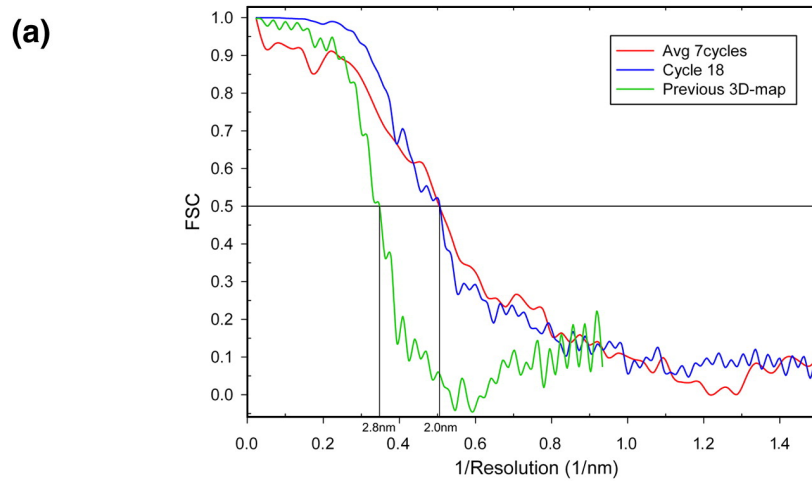
Suppl. Fig. 3. (a) Fourier shell correlation (FSC) calculated using IMAGIC (van Heel, M., Harauz, G., Orlova, E. V., Schmidt, R. & Schatz, M. (1996). A new generation of the IMAGIC image processing system. *J. Struct. Biol.* **116**, 17–24.) for an average of the last 7 cycles of the reconstruction (red line) shown in Fig. 1, and the last 18th cycle (blue line), and our previous reconstruction18 (green line). The 0.5 threshold resolution is 2 nm. (b,c) Example of comparison of three-dimensional reconstructions obtained from the same 5,000 filament segment images: without (a) and with (b) filament tilt correction. In (a), similar to the three-dimensional map reported previously by us18, 1,500 segments were picked up by the IHRSR method, while 2,700 were included using the tilt correction. The new feature 'a' in Fig. 1 revealed in the current reconstruction is seen only with tilt correction, and the feature 'b' is enhanced. (d–f) The current three-dimensional map, unfiltered (d), and filtered at the resolution derived from the FSC (e; 2 nm) or at the theoretical 2.57 nm (f) derived from the corrected −1.95-µm defocus used to record the images (see Supplementary Methods). Note: while the FSC reveals good correspondence between independent reconstructions to 2 nm resolution, this is better than the non-CTF corrected resolution of the original images (limited by the electron optics of the microscope). However, the new features are visible even at this lower resolution filtering (f).

Supplementary Movie:

Complementarity of electrostatic charges of the free and blocked RLC NTFs and the domain 1 of RLC. This movie is based in Fig. 7abc. First, it shows the flexed RLCs in ribbons of the blocked head (orange) and its NTF (yellow), and the free head (magenta) and its NTF (pale green). The ribbons models are then rotated −30° and replaced by their corresponding electrostatic surface charges (blue positive, red negative, white neutral). The free-head NTF is separated, moved to the right and then rotated to show its back surface, which is in front of the domain 1 of RLC and the blocked-head NTF. The complementarity of charges is seen. Then this NTF is returned to its original position. In the second part of the movie, the flexed RLCs in ribbons reappear and are rotated 160°. After that the RLC free head and NTF are removed, leaving only the blocked-head RLC and NTF. The ribbons models are then replaced by their corresponding electrostatic surface charges again. Finally the blocked-head NTF is separated to the right and rotated to show its back surface (which is in contact with only the domain 1 of RLC). The complementarity of charges is seen.

Supplementary Methods:

The resolution of the 3D-reconstruction: The theoretical achievable resolution for the set of electron micrographs used in this work depends on the defocus of each micrograph and other fixed parameters related to the CM-120 microscope used. Although the micrographs were taken at a nominal CM-120 readout defocus of 1.5 µm, there was a range of actual defocus values around the targeted value of 1.5 µm apparent in the set of electron micrographs. Two factors must be taken into account in analyzing these

images, one concerning the actual defocus value (as compared with the nominal readout of 1.5 μm), and the other concerning the actual range of defocus. Concerning the first point, recent calibration of the nominal readout defocus has shown that the defocus readout on the microscope underestimates the true defocus by 23%. Assuming that the focusing for all the filaments was good, the true defocus would have been -1.95 μm, and not the -1.5 μm taken from the CM-120 firmware-based readout. For this defocus value, and for 120 KV and other fixed parameters for the CM-120, the first zero of the CTF evaluated with (de Jong, A. F. & van Dyck, D. (1993). Ultimate resolution and information in electron microscopy: II. The information limit of transmission electron microscopes. (*Ultramicroscopy*, **49**, 66–80.) would occur at ~2.57 nm instead of ~ 2.3 nm for the nominal value of -1.50 μm. This means that features finer than 2.57 nm may be spurious, due to phase flipping. Concerning the second point, in the chosen batch of 89 electron micrographs, the apparent range of defocus implies a mixture of resolutions in the range ~1.8-2.57 nm, such that the final composed resolution of the 3D-map would depend on the number of micrographs corresponding to each defocus value. Unfortunately, it has not been possible to determine the defocus of each micrograph, and therefore we could not perform the required CTF correction. The resolution of the current reconstruction estimated by the Fourier Shell Correlation 0.5 threshold is about 2 nm (suppl. fig. 3a). It is important to remember that the FSC gives an indication of reproducibility of features between two independent reconstructions, but cannot take account of features that are reproducible but nevertheless spurious. As this 2 nm value is better than the theoretical instrumental resolution of 2.57 nm (without CTF correction), finer features could be spurious due to phase flipping. We have therefore determined whether these finer features are actually present, by filtering the reconstruction to this lower level. Suppl. fig. 3def shows that the finer features are indeed also present at this lower resolution. It appears that the better definition of the fine details of the 3D-map is due to the additional structural information and the improved signal-to-noise ratio obtained with the increased number of images in the reconstruction, getting closer to the theoretical averaging plateau, by including the images of the tilted filament segments discarded by the standard IHRSR method.